THE JOURNAL OF BIOLOGICAL CHEMISTRY VOL. 286, NO. 3, pp. 1987–1998, January 21, 2011

Structure and Catalysis of Acylaminoacyl Peptidase

CLOSED AND OPEN SUBUNITS OF A DIMER OLIGOPEPTIDASE[*S]

Received for publication, July 29, 2010, and in revised form, October 25, 2010 Published, JBC Papers in Press, November 16, 2010, DOI 10.1074/jbc.M110.169862

Veronika Harmat[‡1], Klarissza Domokos[§1], Dóra K. Menyhárd[‡], Anna Palló[¶2], Zoltán Szeltner[§], Ilona Szamosi[§], Tamás Beke-Somfai[‡3], Gábor Náray-Szabó[‡], and László Polgár[§4]

From the [‡]Laboratory of Structural Chemistry and Biology and HAS-ELTE Protein Modeling Group, Institute of Chemistry, Eötvös Loránd University, Pázmány P. sétány 1/A, H-1117 Budapest, Hungary, the [§]Institute of Enzymology, Biological Research Center, Hungarian Academy of Sciences, Karolina út 29, H-1113 Budapest, Hungary, and the [¶]Department of Neurochemistry, Chemical Research Center, Hungarian Academy of Sciences, Pusztaszeri ut 59–67, H-1025 Budapest, Hungary

Acylaminoacyl peptidase from *Aeropyrum pernix* is a homodimer that belongs to the prolyl oligopeptidase family. The monomer subunit is composed of one hydrolase and one propeller domain. Previous crystal structure determinations revealed that the propeller domain obstructed the access of substrate to the active site of both subunits. Here we investigated the structure and the kinetics of two mutant enzymes in which the aspartic acid of the catalytic triad was changed to alanine or asparagine. Using different substrates, we have determined the pH dependence of specificity rate constants, the rate-limiting step of catalysis, and the binding of substrates and inhibitors. The catalysis considerably depended both on the kind of mutation and on the nature of the substrate. The results were interpreted in terms of alterations in the position of the catalytic histidine side chain as demonstrated with crystal structure determination of the native and two mutant structures (D524N and D524A). Unexpectedly, in the homodimeric structures, only one subunit displayed the closed form of the enzyme. The other subunit exhibited an open gate to the catalytic site, thus revealing the structural basis that controls the oligopeptidase activity. The open form of the native enzyme displayed the catalytic triad in a distorted, inactive state. The mutations affected the closed, active form of the enzyme, disrupting its catalytic triad. We concluded that the two forms are at equilibrium and the substrates bind by the conformational selection mechanism.

Serine peptidases contain a catalytic triad (serine, histidine, and aspartic acid) that is implicated in bond breaking and bond making (1–3). Although the catalytic roles of serine and histidine are clear, the discovery of hydrogen bond formation between His^{57} and Asp^{102} of chymotrypsin initiated a long discussion concerning the contribution of aspartic acid to the catalysis. It was postulated that the three residues form a charge relay system wherein the proton of the Ser^{195} OH group is mediated by the His^{57} imidazole to the Asp^{102} carboxylate ion (4). This proposal was questioned on the basis of chemical properties of the interacting groups, which renders the proton transfer from the highly basic serine OH group to an acidic carboxyl group unlikely (5). The lack of proton transfer to the aspartate residue was confirmed by NMR (6, 7) and neutron diffraction experiments (8). It was further suggested that the catalytic triad serves as a charge-stabilizing system, where the aspartate ion stabilizes the protonated histidine that interacts with the negatively charged tetrahedral intermediate (1, 9–11). Computational methods were also used to determine the quantitative catalytic contribution of the aspartic acid and other catalytic residues of classical serine proteases (11, 12).

Carter and Wells (13) initiated a comprehensive mutagenesis study on the catalytic triad of subtilisin. This included the substitution of the catalytic aspartic acid for an alanine residue. The mutation reduced the turnover number, having only a minor effect on the Michaelis constant. The specificity rate constant decreased from 27,000 to 4.7 $M^{-1}s^{-1}$.

The role of the catalytic aspartic acid in trypsin catalysis was investigated by substituting Asp^{102} for the neutral Asn^{102} (14, 15). It was concluded from the rate decrease of 4 orders of magnitude and from x-ray crystallographic measurements that the modified enzyme held the tautomer form of His^{57}, which was unable to accept the proton from the serine OH group. Specifically, the Nϵ2 of His^{57} was protonated, and the basic Nδ1 formed a hydrogen bond with the NH_2 group of Asn^{102} (14).

Site-specific mutagenesis was conducted also with POP,[5] a member of a different family of serine peptidases (family S9 of

* This work was supported by grants from the Hungarian Science Fund (OTKA NK67800, F67937, and K72973; European Union FP7 (223077 and 226716); the European Union and the European Social Fund (TÁMOP 4.2.1./B-09/KMR-2010–0003); and the ICTP-ELETTRA Users Programme.

[S] The on-line version of this article (available at http://www.jbc.org) contains supplemental Table S1.

The atomic coordinates and structure factors (codes 3O4G, 3O4H, 3O4I, and 3O4J) have been deposited in the Protein Data Bank, Research Collaboratory for Structural Bioinformatics, Rutgers University, New Brunswick, NJ (http://www.rcsb.org/).

[1] Both authors contributed equally to this work.

[2] Present address: Inst. of Structural Chemistry, Chemical Research Center, Hungarian Academy of Sciences, Pusztaszeri ut 59–67, H-1025 Budapest, Hungary.

[3] Present address: Dept. of Chemical and Biological Engineering and Physical Chemistry, Chalmers University of Technology, SE-412 96 Göteborg, Sweden.

[4] To whom correspondence should be addressed: Inst. of Enzymology, Biological Research Center, Hungarian Academy of Sciences, P. O. Box 7, H-1518 Budapest, Hungary. Tel.: 36-1-279-3110; Fax: 36-1-466-5465; E-mail: polgar@enzim.hu.

[5] The abbreviations used are: POP, prolyl oligopeptidase; AAP, acylaminoacyl peptidase; ApAAP, *Aeropyrum pernix* K1 AAP; Abz, 2-aminobenzoyl; Nap, 2-naphthylamide; ONp, 4-nitrophenyl; Phe(NO_2), 4-nitrophenylalanine; Taps, 3-{[2-hydroxy-1,1-bis(hydroxymethyl)ethyl]amino}-1-propanesulfonic acid; r.m.s., root mean square; PDB, Protein Data Bank.

clan SC), unrelated to the classic trypsin and subtilisin families. Two variants, D641N and D641A, were examined. With the use of the alanine variant, the proper stabilization of the unfavorable tautomer form of the catalytic histidine was excluded. Kinetic investigations indicated that the contribution of the catalytic aspartic acid was very much dependent on the substrate leaving group and other factors (16).

The crystal structure of POP was the first reported in family S9 (17). It was shown that the enzyme contains a peptidase domain with α/β hydrolase fold and that its catalytic triad ($Ser^{554}/Asp^{641}/His^{680}$) is covered by the central tunnel of a seven-bladed β-propeller. This domain makes the enzyme an oligopeptidase by excluding large, structured peptides from the active site. In this way, the propeller protects large peptides and proteins from proteolysis in the cytosol.

Mammalian acylaminoacyl peptidase (AAP), a member of the POP family, is an exopeptidase, which removes acylated amino acid residues from the N terminus of oligopeptides. A deficiency in human AAP has been linked with small cell lung carcinoma and renal cell carcinoma (18–20), whereas the inhibition of the enzyme has led to apoptosis (21). AAP is a more sensitive target than acetylcholinesterase for certain organophosphorus compounds, and thus it may be a potential site for cognition-enhancing drugs (22, 23).

The crystal structure of the mammalian AAP is unknown. Only the structure of AAP from the thermophile *Aeropyrum pernix* K1 (ApAAP) has been reported (24, 25). Unlike the tetramer mammalian enzyme, ApAAP is a symmetrical homodimer with each subunit containing two domains, an N-terminal seven-bladed β-propeller and a peptidase domain with α/β-hydrolase fold, which are characteristic of this enzyme family. The catalytic triad of ApAAP consists of the Ser^{445}, Asp^{524}, and His^{556} residues. The structure determinations of various enzyme-inhibitor complexes delineated the hydrophobic S1 substrate binding pocket that accepts large nonpolar residues, like phenylalanine and leucine (24, 25). This binding site is different from that of the porcine enzyme, which is specific for the small alanine side chain. Kinetic analysis using various peptide substrates have revealed that ApAAP, which was regarded as an exopeptidase, exhibits endopeptidase activity as well (25).

Herein, the effects of mutations on the active site of ApAAP were investigated under various reaction conditions with different substrates. The catalytic Asp^{524} was mutated to asparagine and alanine, which resulted in catalytic behaviors different from that of trypsin or POP. The structural consequences of mutation were demonstrated by crystal structure determination, which also revealed conformational changes associated with the oligopeptidase activity. The kinetic and structural results support the conformational selection mechanism for ligand binding rather than the induced-fit mechanism.

EXPERIMENTAL PROCEDURES

Mutagenesis of ApAAP—The ApAAP gene (*APE1547*) (25) was amplified by PCR using the primers 5′-GTTAGAC-CATATGCGCATTATAATGCCTGT-3′ (sense, NdeI restriction site underlined) and 5′-AGTTTGGATCCTCATCTC-CTCTCCCTCTGG-3′ (antisense, BamHI restriction site underlined).

Mutations were introduced with the two-step PCR method described for the H507A variant of porcine AAP (26). The mutagenic primer pair for the D524A variant consisted of 5′-CCTCAGAACGctAGCAGAACACC-3′ (sense) and 5′-GGTGTTCTGCTagCGTTCTGAGG-3′ (antisense). For the D524N mutation, the two primers were 5′-CCTCAGAACaA-CAGCAGAACACC-3′ (sense) and 5′-GGTGTTCTGCTGTt-GTTCTGAGG-3′ (antisense). (Lowercase letters designate the mutated nucleotides.) The amplified gene products were digested with BamHI and NdeI restriction endonucleases and ligated to a pET22b vector opened with the same restriction enzymes. The constructs were sequenced.

Preparation of ApAAP Enzymes—The same method was applied for preparation of the D524A and D524N variants as described for the wild-type enzyme (25). The protein concentration of the monomer enzyme was calculated from the absorbance at 280 nm using a value of 63.03 kDa and A_{280} (0.1%) = 0.93.

Enzyme Kinetics—The reaction of ApAAP with Ac-Phe-Nap was measured fluorometrically, using a Cary Eclipse fluorescence spectrophotometer equipped with Peltier four-position multicell holder accessory and temperature controller. The excitation and emission wavelengths were 340 and 410 nm, respectively. The substrate with intrinsically quenched fluorescence, Abz-Ala-Leu-Phe-Gln-Gly-Pro-Phe(NO_2)-Ala, was prepared with solid phase synthesis, and its hydrolysis was measured fluorometrically as with Ac-Phe-Nap, except that the excitation and emission wavelengths were 337 and 420 nm, respectively. The liberation of 4-nitrophenyl from caprylic-ONp (caprylic acid 4-nitrophenyl ester, Fluka) was monitored spectrophotometrically at 400 nm. The reactions were measured at 70 °C in a universal buffer containing 30 mM Mes, 30 mM Hepes, 30 mM Taps, 30 mM glycine, 1% dimethyl sulfoxide, and 0.3 M NaCl. A relatively high concentration of dimethyl sulfoxide was applied because of the poor solubility of some substrates. At this concentration, the organic solvent did not affect the kinetics.

The pseudo-first-order rate constants were measured at substrate concentrations lower than 0.1 K_m and calculated by nonlinear regression data analysis using GraFit software (27). The specificity rate constant (k_{cat}/K_m) was obtained by dividing the first-order rate constant by the total enzyme concentration in the reaction mixture.

For the calculation of pH dependence curves, GraFit software was used (27). The Michaelis-Menten parameters (k_{cat} and K_m) were determined with initial rate measurements using substrate concentrations in the range of 0.2 to 5 K_m. The kinetic parameters were calculated with nonlinear regression analysis.

Determination of Dissociation Constants of Enzyme-Substrate and Enzyme-inhibitor Complexes—The dissociation constant (K_s) of the oligopeptide, an intrinsically quenched substrate, was determined from the fluorescence change that occurred upon substrate binding to the inactive S445A variant of ApAAP. Equation 1 (28) describes the formation of the enzyme-substrate complex (*ES*) at similar concentrations of *E*

and S, when the conditions for the Michaelis-Menten equation do not meet.

$$ES = [(S_0 + E + K_s) - \sqrt{(S_0 + E + K_s)^2 - 4E^*S_0}]/2 \quad \text{(Eq. 1)}$$

$$\Delta F = \Delta F_{max}[(S_0 + E + K_s) - \sqrt{(S_0 + E + K_s)^2 - 4E^*S_0}]/2S_0 \quad \text{(Eq. 2)}$$

The substrate (S_0) was saturated with increasing amounts of enzyme (E). Although ES is not known, its concentration is proportional to the change in the fluorescence signal measured at 328 and 420 nm excitation and emission wavelengths, respectively. Hence, Equation 1 can be transformed into Equation 2, where ΔF corresponds to ES and ΔF_{max} gives the change in signal when the substrate is completely converted into the enzyme-substrate complex. A plot of ΔF against E gives K_s and ΔF_{max} using nonlinear regression.

The K_i values for Ac-Phe-OH, the dissociation constants of the enzyme-inhibitor complex, were calculated from Equation 3, where k_i and k_0 are pseudo-first-order rate constants determined at substrate concentrations of $<0.1\ K_m$ in the presence and absence of inhibitor (I), respectively (16, 25).

$$k_i/k_0 = 1/(1 + I/K_i) \quad \text{(Eq. 3)}$$

Crystallographic Studies—All protein samples were crystallized at room temperature using the hanging drop method. Crystals of native ApAAP and the D524A mutant were grown from 78 mM sodium acetate buffer, pH 5.5, except for the double open form, which crystallized only at pH 4.5. The buffer also contained 0.44 mM EDTA, 2.0–2.4% PEG (M_r 4000), and 6.7 mM dithiothreitol. The protein solution contained 0.19–0.29 mM ApAAP in 20 mM Tris buffer, pH 8.0. The crystallization of the D524N form was carried out using 170 mM sodium acetate buffer, pH 5.0, containing 0.40 mM EDTA, 2.5% PEG (M_r 4000), and 10% dimethyl sulfoxide. The protein solution contained 0.14 mM ApAAP in 20 mM Tris buffer, pH 8.0, and 30 mM NaCl. Crystallization drops were composed of 2–3 μl of protein solution and 2 μl of reservoir solution. An additional compound in the crystallization drops of the native enzyme was phenylboronic acid, whereas in the case of the D524A "open/open" crystal form, agarose gel and β-octyl glucoside were added. These compounds did not associate with the enzyme in the crystalline state. The details of the crystallization conditions are compiled in supplemental Table S1. Glycerol was used as a cryoprotectant.

Data collection was carried out by synchrotron radiation at EMBL/DESY Hamburg using beamline X11 (the D524A "open/closed" form and D524N form) as well as beamline X12 (native enzyme). Data of the D524A open/open form was collected at the ELETTRA synchrotron source at beamline XRD1. Data processing and data reduction were carried out with the XDS and XSCALE programs (29).

The enzyme structures were solved by molecular replacement using the MOLREP program (30) of Collaborative Computing Project 4 (CCP4). The hydrolase and propeller domains of the uncomplexed enzyme were used as a search model (PDB ID code 1VE6) (24). Refinement was carried out with the REFMAC5 program (31) using restrained maximum likelihood refinement and TLS refinement (32). During refinement noncrystallographic restraints were added to the respective domains of ApAAP molecules possessing similar conformation (*i.e.* with both open or both closed). Model building was carried out using the Coot program (33).

$$E + S \underset{k_{-1}}{\overset{k_1}{\rightleftharpoons}} ES \xrightarrow{k_2} EA \xrightarrow{k_3} E$$
$$\qquad\qquad\qquad\qquad\quad P_1 \qquad\qquad P_2$$

SCHEME 1

The stereochemistry of the structures was assessed with PROCHECK (34). The atomic coordinates and structure factors were deposited in the Protein Data Bank (35). Figs. 5 and 6 were created using PyMOL (36). Protein-protein interfaces were analyzed using the PROTORP server (37).

RESULTS

The pH Rate Profile of k_{cat}/K_m Markedly Changes with the Mutant Enzymes—Hydrolysis by serine peptidases proceeded with the formation of an acyl-enzyme intermediate as shown in Scheme 1, where E, S, ES, EA, P_1, and P_2 are the free enzyme, the substrate, the enzyme-substrate complex, the acyl-enzyme, the leaving group of S, and the acyl moiety of S, respectively. The rate constants k_1, k_{-1}, k_2, and k_3 stand for the formation of ES, the dissociation of ES, and first-order acylation and deacylation, respectively. The second-order acylation rate constant, also called the specificity rate constant (k_{cat}/K_m), involves both binding ($K_s = k_{-1}/k_1$) and acylation (k_2) but not deacylation (k_3) (38). The process depicted in the first part of Scheme 1 represents the second-order acylation: $E + S \rightarrow EA + P_1$.

Asp^{524} of ApAAP interacts with the catalytic His^{556} through a hydrogen bond. The importance of interaction was studied with the aid of the D524A and D524N enzyme variants. In the absence of the hydrogen bond (D524A) and the negative charge (D524N), the pH dependence of the specificity rate constant (k_{cat}/K_m) may furnish useful mechanistic information about the change in the protonation state of His^{556}. Fig. 1*A* illustrates the pH-k_{cat}/K_m profile of the reaction of the wild-type ApAAP and its variants with Ac-Phe-Nap. The wild-type enzyme exhibits a bell-shaped pH-rate profile, whereas the rate constants for the D524A and D524N variants increase to about pH 9. The protein tends to unfold above this pH level, as shown below. As shown in Table 1 the k_{cat}/K_m values are much lower compared with those of the wild-type enzyme. At pH 7.0 the ratios of k_{cat}/K_m are 2090 and 660 for the wild-type/D524A and wild-type/D524N variants, respectively.

The experimental points for the D524A variant conform to a double sigmoid curve. Importantly, the pK_1 values for the wild-type enzyme and the D524A variant are similar (Table 1). This implies that the lower sigmoid part of the curve for the modified enzyme may correspond to the ascendant limb of the bell-shaped curve obtained with the wild-type enzyme. Above pH ~7 the electrostatic environment around the active

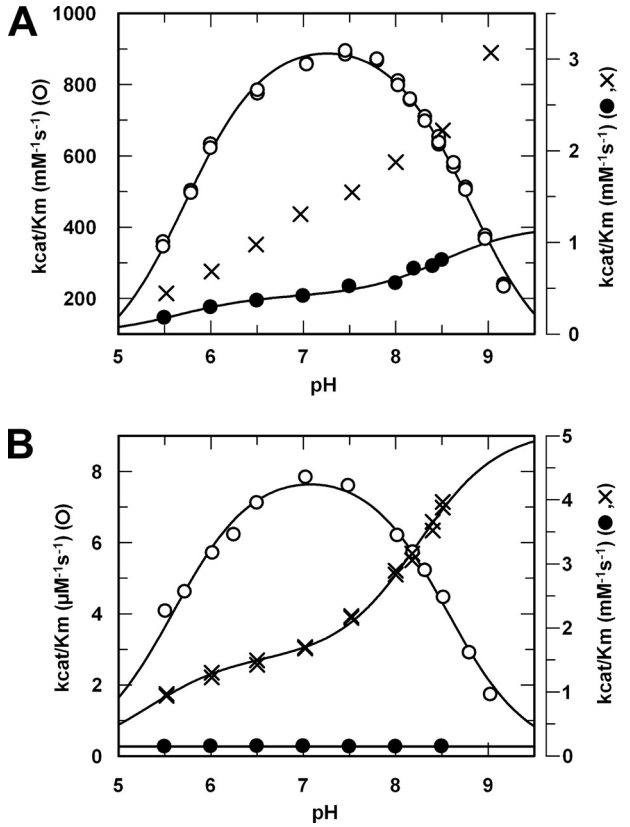

FIGURE 1. **pH dependence in the reactions of Ac-Phe-Nap with ApAAP and its variants, D524A and D524N.** *A*, the substrate is Ac-Phe-Nap. *Circles*, *full circles*, and *crosses*, refer to ApAAP, the D524A variant, and the D524N variant, respectively. The *lines* for the wild-type and the D524A variant represent bell-shaped and doubly sigmoid curves, respectively. The parameters for the curves are shown in Table 1. *B*, the substrate is Abz-Ala-Leu-Phe-Gln-Gly-Pro-Phe(NO_2)-Ala. The signs for the enzymes are identical with those shown in *A*.

TABLE 1

Kinetic parameters extracted from the pH-rate profiles of ApAAP and its variants

Substrate/ enzyme	k_{cat}/K_m (limit)$_1$	k_{cat}/K_m (limit)$_2$	pK_1	pK_2
	$mM^{-1}s^{-1}$	$mM^{-1}s^{-1}$		
Ac-Phe-Nap				
Wild type	939 ± 8		5.72 ± 0.02	8.80 ± 0.01
D524A	0.419 ± 0.038	1.18 ± 0.35	5.65 ± 0.17	8.49 ± 0.38
D524N[a]				
Oligopeptide				
Wild type	8130 ± 195		5.60 ± 0.04	8.56 ± 0.04
D524A[b]	0.146 ± 0.023			
D524N	1.527 ± 0.052	5.100 ± 0.225	5.33 ± 0.08	8.24 ± 0.07

[a] Cannot be fit.
[b] Practically pH independent (see Fig. 1*B*).

site changes progressively with the increase in pH, and this impairs the catalytic machinery. Although this effect is unfavorable for the wild-type enzyme, it facilitates the hydrolytic activity of the mutant enzymes of reduced activity. The D524N variant may also have acidic and alkaline pH forms, but the two forms are not sufficiently separated to fit a double sigmoid curve properly to the points.

In addition to the exopeptidase activity measured with Ac-Phe-Nap, the endopeptidase activity of ApAAP was also examined using the oligopeptide substrate Abz-Ala-Leu-Phe-Gln-Gly-Pro-Phe(NO_2)-Ala, in which the Phe-Gln bond was

TABLE 2

Kinetic parameters for the reactions of ApAAP and its variants at pH = 7.0

Substrate/ enzyme	Wild type	D524A	D524N
Ac-Phe-Nap			
k_{cat} (s^{-1})	4.28 ± 0.17		
K_m (μM)	5.66 ± 0.50	>80	>30
k_{cat}/K_m ($mM^{-1}s^{-1}$)	756 ± 73		
k_{cat}/K_m ($mM^{-1}s^{-1}$)[a]	865 ± 15	0.414 ± 0.011 (2090)[b]	1.31 ± 0.05 (660)[b]
Oligopeptide[c]			
k_{cat} (s^{-1})	8.188 ± 0.324	0.000917 ± 0.000087	0.00525 ± 0.00024
K_m (μM)	1.29 ± 0.11	7.1 ± 1.1	2.81 ± 0.31
k_{cat}/K_m ($mM^{-1}s^{-1}$)	6347 ± 597	0.129 ± 0.023	1.87 ± 0.22
k_{cat}/K_m ($mM^{-1}s^{-1}$)[a]	7800 ± 120	0.146 ± 0.002 (53425)[b]	1.728 ± 0.023 (4514)[b]
K_s (μM)[d]	0.807 ± 0.037	1.04 ± 0.11	0.781 ± 0.028
Caprylic-ONp			
k_{cat} (s^{-1})	8.67 ± 0.70	0.0313 ± 0.0027	0.0320 ± 0.0017
K_m (μM)	23.2 ± 3.7	26.6 ± 4.2	11.7 ± 1.7
k_{cat}/K_m ($mM^{-1}s^{-1}$)	374 ± 67	1.18 ± 0.21	2.74 ± 0.42

[a] Measured under first-order conditions.
[b] Ratios of the rate constants for the wild-type and mutant enzymes are shown in parentheses.
[c] Abz-Ala-Leu-Phe-Gln-Gly-Pro-Phe(NO_2)-Ala.
[d] Measured with the S445A, S445A/D524N, and S445A/D524A variants.

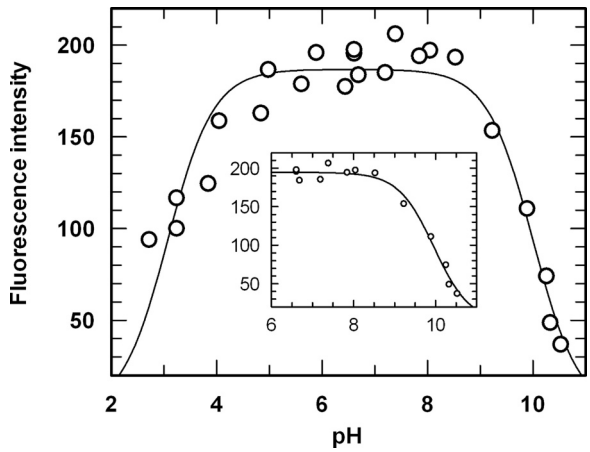

FIGURE 2. **pH dependence of intrinsic fluorescence of ApAAP.** Fluorescence intensity at 0.372 μM enzyme was measured at 70 °C and shown in arbitrary units. The excitation and emission wavelengths are 280 and 335 nm. A bell-shaped curve was fit to the points. The *insert* shows the fit of a sigmoid curve with a pK_a of 9.96 ± 0.05 at the alkaline side.

cleaved. The oligopeptide substrate also exhibited a bell-shaped pH-rate profile for the wild-type enzyme and increasing k_{cat}/K_m for the D524N variant (Fig. 1*B* and Table 1). However, the rate constant for the D524A variant was practically independent of pH. The reductions in k_{cat}/K_m for the mutated enzymes are significantly greater with the more specific oligopeptide than with the Ac-Phe-Nap, as seen in Table 2. This is mostly because of the decrease in k_{cat} and, to a lesser extent, the increase in K_m. For solubility reasons, the exact K_m and k_{cat} of the Ac-Phe-Nap reactions could not be determined for the mutant enzymes. It is noteworthy that the wild-type enzyme displayed a kinetic specificity higher by 1 order of magnitude for the oligopeptide than for the Ac-Phe-Nap substrate (7800 *versus* 865 $mM^{-1}s^{-1}$ (Table 2)).

Above pH 9.0 the k_{cat}/K_m decreased sharply with the mutant enzymes. This may have been because of conformational changes in the protein structure. To address this point, we used a simple fluorometric method, which demonstrated that the intrinsic fluorescence decreased at moderate acidic and alkaline pH values (Fig. 2), confirming the expected confor-

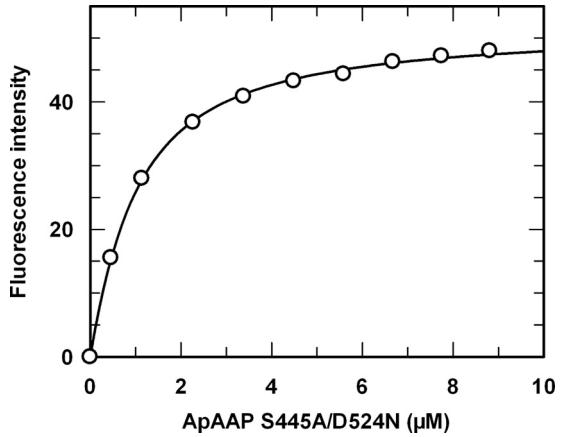

FIGURE 3. **Determination of K_s for the Abz-Ala-Leu-Phe-Gln-Gly-Pro-Phe(NO_2)-Ala-APAAP(S445A/D524A) complex.** 0.2 μM substrate was titrated with increasing amounts of enzyme.

mational changes in protein structure. The overall structure of the enzyme was stable in the pH range between 4.5 and 8.5. In the alkaline pH region the unfolding was controlled by a single ionization (Fig. 2, *insert*), whereas on the acidic side, the fluorescence decrease conformed to multiple ionizations.

The Binding Strengths of the Oligopeptide are Similar for the Wild-type and Modified ApAAPs—The oligopeptide as an intrinsically quenched substrate rendered it feasible to determine the dissociation constant of the enzyme-substrate complex ($K_s = k_{-1}/k_1$) (16). This allowed us to reveal possible changes in the value of K_s arising from modification of the catalytic aspartic acid. To this end, the inactive variants of ApAAP (S445A, S445A/D524N, and S445A/D524A), which bind but do not hydrolyze the substrate, were used. Fig. 3 illustrates the titration of the oligopeptide substrate with increasing amounts of the S445A/D524N variant of ApAAP. Using the same method, the K_s values were identical with that of the S445A enzyme, whereas that of the S445A/D524A mutant was slightly higher (weaker binding) (Table 2). This indicated that the modification of the catalytic aspartate residue did not appreciably affect the binding of the oligopeptide.

The large oligopeptide interacts with the different enzymes at multiple subsites, at least five or six. This explains why the binding represented by the equilibrium constant, K_s, does not depend very much on mutation but rather depends on the acylation constant, k_2. The binding is not significantly affected by the pH either, as indicated by our measurements at pH 5.5 (not shown). However, we prefer the results obtained near the physiological pH of 7.0, because the catalytic histidine becomes partially doubly protonated at pH 5.5. Moreover, at the lower pH, the protein starts to unfold.

Table 2 indicates that K_s is close to the K_m for the native enzyme reacting with the oligopeptide. This occurs when $k_2 < k_{-1}$, and thus $K_m = (k_2 + k_{-1})/k_1$ is simplified to $K_m = k_{-1}/k_1$. Although the K_m value does not change severely for the oligopeptide, it increases considerably for the Ac-Phe-Nap substrate. The dissimilarity can be explained in terms of $K_m = (k_2 + k_{-1})/k_1 = K_s + k_2/k_1$, which indicates that K_m may be greater than K_s by the value of k_2/k_1, as found in the hydrolysis of Ac-Phe-Nap catalyzed by the mutant enzymes (Table 2). In the oligopeptidase reactions the decrease in k_{cat}/K_m for the mutant enzymes principally depends on the reduction in k_{cat} rather than on the increase in K_m. As k_{cat}/K_m is equal to k_2/K_s (38, 39), the k_{cat} should be similar to k_2.

In addition to cleaving the peptide bond, serine peptidases also hydrolyze the more reactive ester bond. Thus, 4-nitrophenyl caprylate is a good substrate for ApAAP (40). Table 2 shows that the values of k_{cat}/K_m for the mutant enzyme reactions diminished by 2 orders of magnitude. As K_m is practically unchanged, the decrease in k_{cat} accounts for the reduction in the specificity rate constant. In this respect, the reaction of caprylic-ONp resembles that of the oligopeptide, but the decrease in k_{cat} is much greater with the oligopeptide.

Formation of the ApAAP-Ac-Phe-4-nitroanilide Complex is the Rate-limiting Step in Acylation—The second-order acylation rate constant (k_{cat}/K_m) is dependent on the strength of the chemical bond to be cleaved, if the chemical step (k_2) is rate-limiting. On the other hand, the effect of the leaving group is not significant if a physical step, *e.g.* conformational change or substrate binding, controls the catalysis. A classical example is the acylation of chymotrypsin, which is faster by 6 orders of magnitude with a 4-nitrophenyl ester substrate than with the corresponding amide (41). Obviously, the great difference between the nitrophenyl ester and the corresponding amide manifests itself in acylation and indicates that the chemical reaction is the rate-limiting step. In contrast, we obtained relatively similar rate constants for the wild-type ApAAP, namely 0.56 and 1.48 $\mu M^{-1}s^{-1}$ using Ac-Phe-4-nitroanilide, and Ac-Phe-ONp, respectively. The similarity of the rate constants indicates that the rate-limiting step is not a chemical but rather a physical step that is characterized by k_1. Similar results have been obtained previously with the porcine POP (42). Unfortunately, the rate constants for the ApAAP variants could not be determined because of the high spontaneous hydrolysis of the ester substrate relative to the very low rates of hydrolysis with the mutant enzymes.

Titration with the Ac-Phe-OH Inhibitor Indicates that Participation of the Catalytic Histidine is Different in the Reactions of Different ApAAP Variants—We have demonstrated previously that the product-like inhibitor Ac-Phe-OH forms a complex with the wild-type ApAAP (25). The association constant ($1/K_i$) of the enzyme-inhibitor complex increased with the decrease in pH, as the catalytic His^{556} became protonated, which facilitated the electrostatic interaction between the enzyme and the carboxylate ion of the inhibitor. Fig. 4 and Table 3 show the titration curves and the pK_a values of the wild-type enzyme (6.16) and its D524N variant (6.21). It should be noted that the maximum association constants are extrapolated values; however, the errors are reasonable (Table 3). These pK_a values are somewhat higher than those extracted from the pH dependence curve for the wild-type enzyme (5.72) and the D524N variant (5.65) in the reaction with Ac-Phe-Nap. In contrast to the Ac-Phe-Nap, the Ac-Phe-OH does not bind in catalytically competent form, as indicated by crystal structure determination (25). Although one of the oxygen atoms of the carboxylate ion is located in the oxyanion hole, the other oxygen is too far from the protonated imidazole to establish a salt bridge. The distances in monomer A

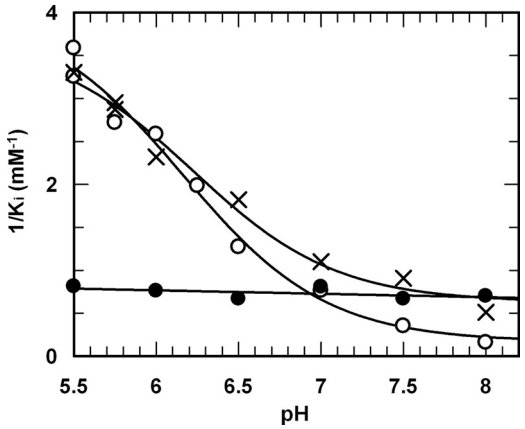

FIGURE 4. **pH dependence of $1/K_i$ for the complex of Ac-Phe-OH formed with ApAAP and its variants.** The *circle* and the *cross* represent the wild-type and the D524N variant, respectively. The *full circle* refers to the D524A variant. The parameters for the curves are shown in Table 3. The first-order rate constants were measured with Ac-Phe-Nap.

TABLE 3

Association constants ($1/K_i$) for the complex of Ac-Phe-OH formed with ApAAP and its variants

Parameters of pH rate profiles	Wild type[a]	D524A	D524N
pK_a	6.16 ± 0.10	pH-independent	6.21 ± 0.15
$1/K_i$ for the low pH form (1/mM)	4.06 ± 0.24	0.79 ± 0.05	3.56 ± 0.30
$1/K_i$ for the high pH form (1/mM)	0.17 ± 0.12	0.70 ± 0.05	0.68 ± 0.16

and monomer B are 5.04 and 5.12 Å, respectively (25), unlike other serine peptidase-product-like inhibitor complexes, where normal hydrogen bonds are formed (43, 44). Unexpectedly, the pK_a for the D524A enzyme cannot be determined, because the association constant is practically independent of pH. This indicates that protonation of His^{556} does not facilitate the binding of Ac-Phe-OH.

Crystal Structures of Native ApAAP and Its D524A and D524N Mutants Reveal Open and Closed States—Four independent crystal structures were determined, those of the native ApAAP, the D524N mutant, and two different crystal forms of the D524A mutant (crystallographic data are compiled in Table 4). The crystals were grown under similar conditions but at slightly different pHs and protein concentrations, which might account for the different crystal forms. The structures are all homodimeric. However, in three cases (native and D524A and D524N mutants) the dimers are composed of two structurally distinct states, *i.e.* open and closed forms (Fig. 5*A*). The closed form is equivalent to that described previously with an intact active site, which is capable of binding substrate analog or product molecules (24, 25). In the open conformer, the two domains move away to form an opening of about 30°, with Asp^{376} being the hinge (the origin of the opening angle) (Fig. 5*B*). Although the two covalent linkers between the two domains are at the starting point of blade 1 and the end point of blade 7 of the propeller, the hinge point hydrogen bond network is formed by Asp^{376} and the loops of blades 6 and 7. This is the first time that such a mixed homodimer was found. The fourth crystal structure, a D524A mutant, contains both subunits in the open form. Three of the four crystal structures contain two dimers, which are crystallographically independent yet conformationally very similar (open/closed conformation; see also Table 4). The four monomers of these two dimers are referred to as chains A, B, C, and D. Thus, eight crystallographically independent open monomers (chains A and B of the open/open dimer of the D524A mutant, as well as chains B and D of the three crystal structures containing the open/closed mixed homodimers), and six closed forms (chains A and C of the open/closed mixed homodimers) were obtained.

Note that most crystals of ApAAP were grown at slightly acidic pH (Refs. 24 and 25 and this study), but as seen in Fig. 2, even at these pH values the enzyme is predominantly in its stable, folded conformation. Previous crystallographic results also support the view that the overall fold and active site conformation is unaffected by the acidic medium, although the catalytic histidine residue may be partially or completely protonated in these structures (25).

A number of interdomain H-bonds stabilize the closed form. These contacts are, almost exclusively, loop-loop-type interactions, whereas the β-sheet and the α-helical regions forming the cores of the two domains mainly have intradomain nonpolar contacts and H-bonds (Fig. 5*B*). Most significantly, loop-(521–529) and loop-(551–560) of the hydrolase domain, which hold the catalytic Asp^{524} and His^{556}, respectively, are linked to loop-(43–46) and loop-(83–88) of the propeller by five H-bonds.

Mutations do not affect the overall structure of either state. The Cα r.m.s. deviations among the closed molecules of the native ApAAP, the D524A and the D524N mutants range from 0.29 to 0.51 Å, whereas the same comparison in the case of the open forms results in Cα r.m.s. deviations between 0.47 to 0.63 Å. The domains themselves are unperturbed by the opening of the molecule. The average Cα r.m.s. deviations between the hydrolase domains in the open and closed forms are 1.0 and 1.1 Å, respectively, whereas the propeller domain proved to be even more conserved, with 0.9 and 1.0 Å r.m.s. deviations, taking into account both the native and the mutant structures.

A comparison of the closed/closed ApAAP dimer structures published previously (24, 25) with the present open/closed and open/open dimers revealed that the conformation of one molecule within the ApAAP dimer is practically independent of the conformation of the other. This indicates that the two monomers act independently and that the dimerization may serve as structure stabilization.

The average backbone B-factors of the individual domains are quite similar in the open and the closed forms. We also compared the relative average B-factors of the loops (average backbone B-factor of the loop, divided by the average B-value of the corresponding domain) in the open and closed states. Opening causes marked liberation of loop-(551–560) containing His^{556}, with an increase of 40–50% in the average B-factor. In the case of loop-(521–529), which contains the site of mutation, the enhancement of B-factors is within the range of 20–30% (Fig. 5*C*).

Effect of Opening on the Active Site Structure—In the native, closed structure, the residues of the catalytic triad are fixed by numerous interactions. The two loops containing Asp^{524} and His^{556} are connected by three H-bonds (Gln^{522}–Ile^{551},

TABLE 4
Data collection and refinement statistics for ApAAP wild-type, D524A, and D524N mutant structures

ApAAP form				
Mutation		D524A	D524A	D524N
Monomer conformation in the dimer	Closed/Open	Closed/Open	Open/Open	Closed/Open
No. of dimers/asymmetric unit	2	2	1	2
Data collection				
Radiation source	DESY, X12	DESY, X11	ELETTRA, XRD1 0.9999	DESY, X11
Wavelength (Å)	0.9786	0.8148		0.8148
Crystal parameters			C222	
Space group	P1	P1	103.632	C2
Cell constants				
a (Å)	71.212	71.405	209.893	184.27
b (Å)	97.016	97.949	205.921	227.524
c (Å)	109.494	98.797	90	110.684
α (°)	89.01	105.687	90	90
β (°)	109.20	103.517	90	100.373
γ (°)	100.21	100.358		90
Data quality				
Resolution range	20.0–2.50	20.0–1.82	20.0–2.70	20.0–2.50
Last shell	2.56–2.50	1.87–1.82	2.77–2.70	2.60–2.50
R_{meas}[a]	0.089 (0.595)	0.028 (0.606)	0.094 (0.527)	0.092 (0.642)
Completeness[a] (%)	94.1 (94.9)	95.2 (94.1)	99.3 (99.8)	96.8 (98.8)
No. observed/unique	176,823/88,675	389,179/206,854	365,256/61,532	493,590/149,375
Last shell[a]	(13,228/6,634)	(28,545/15,188)	(28,471/4,545)	(55,264/16,732)
$I/\sigma(I)$[a]	12.55 (2.01)	22.72 (2.26)	13.20 (3.30)	11.43 (2.48)
Refinement				
R	0.218	0.205	0.209	0.201
R_{free}[b]	0.262	0.234	0.252	0.236
Model quality				
r.m.s. bond lengths (Å)	0.010	0.020	0.019	0.022
r.m.s. bond angles (°)	1.218	1.751	1.764	1.748
r.m.s. general planes (Å)	0.005	0.007	0.008	0.008
Ramachandran plot				
No. of residues in favored/allowed/disallowed regions	1,685/218/2	1,728/1,75/2	845/113/0	1715/193/0
Average B-factor	45.20	44.94	52.86	42.20
Model contents				
No. of residues: protein/water/other	2,302/340/4	2,302/929/7	1,153/335/7	2,307/535/8
No. of atoms: protein/water/other	17,159/340/24	17,201/929/38	8,595/335/37	17,553/535/33
PDB ID	3O4G	3O4H	3O4I	3O4J

[a] Values for the last resolution shell are in parentheses.
[b] 5.0% of the reflections in a test set are for monitoring the refinement process.

Gln^{522}–Asp^{553}, and Asn^{523}–Ala^{554}), besides the catalytically significant Asp^{524} Oδ2–His^{556} Nδ1 interaction. The Oγ atom of Thr^{527} and the backbone nitrogen atoms of Arg^{526} and Thr^{527} are also within H-bonding distance from Oδ1 of Asp^{524}. Besides the Ser^{445} Oγ—His^{556} Nϵ2 contact, the OH group of the neighboring Tyr^{444} residue and the backbone amide nitrogen of His^{556} form an additional H-bond (Fig. 6*A*).

Opening of the structure reorganizes both the loop with residue 524 and, particularly, the loop holding His^{556} (Figs. 5*C* and 6*B*). Loop-(521–529) is merely shifted in the open structures, remaining a well ordered region. In contrast, loop-(551–560) undergoes a major conformational change and becomes entirely exposed to solvent. Although this loop is not well resolved in the electron density maps because of its enhanced flexibility, its backbone trace is visible and quite similar in all open structures. The Cα atom of the catalytic histidine (His^{556}) is moved by 3.4–5.0 Å in the different structures. The effect can be best followed in the open/closed structure of the D524A mutant displaying the highest resolution (1.82 Å). Two interdomain H-bonds (Asn^{559}–Val^{46} and Asn^{559}–Ile^{64}) are replaced by two intradomain (Asn^{559}–Asp^{563} and Thr^{560}–Asp^{563}) interactions in the open structure, whereas the Gly^{44}–Met^{561} main chain interaction is switched to that of the backbone amide nitrogen of Met^{561} and the side chain carboxylate of Glu^{43}. The latter rearrangement causes a shift of more than 4 Å in the end point of loop-(551–560) of all structures, as measured at the Cα atom of Thr^{560} (Fig. 6*B*).

Mutations Cause Distortion in the Active Site Structure of the Closed Form—Although mutations do not cause significant overall changes in either the closed or the open form, the catalytic region of the active, closed form is modified. Interestingly this modification is different from that of POP (16), where the loop structures are altered at the catalytic site. In ApAAP, the backbone conformation is only slightly affected by mutation, whereas the hydrogen bond network of the catalytic triad is considerably perturbed because of significant side chain conformational changes. In the D524A mutant, a water molecule is bound to Nδ1 of His^{556}, near but not exactly at the position of Oδ1 of the replaced carboxylate. As a result, the imidazole of His^{556} is pushed away from the active Ser, increasing the distance between Ser Oγ and His Nϵ2 by more than 0.7Å. The H-bond between the backbone oxygen of His^{556} and the OH group of Tyr^{444} is also lost. The imidazole of His^{556} is forced closer to the guanidinium group of Arg^{526}, decreasing their distance from 4.8 to 4.0 Å (Fig. 6*C*). Arg^{526} plays a key role in substrate binding by interacting with the carbonyl oxygen atom of the substrate (25). The guanidinium moiety of Arg^{526} is bound by an interdomain salt bridge to Glu^{88} of the propeller domain (Fig. 6*C*). The conformational freedom of Arg^{526} is considerably enhanced in the open con-

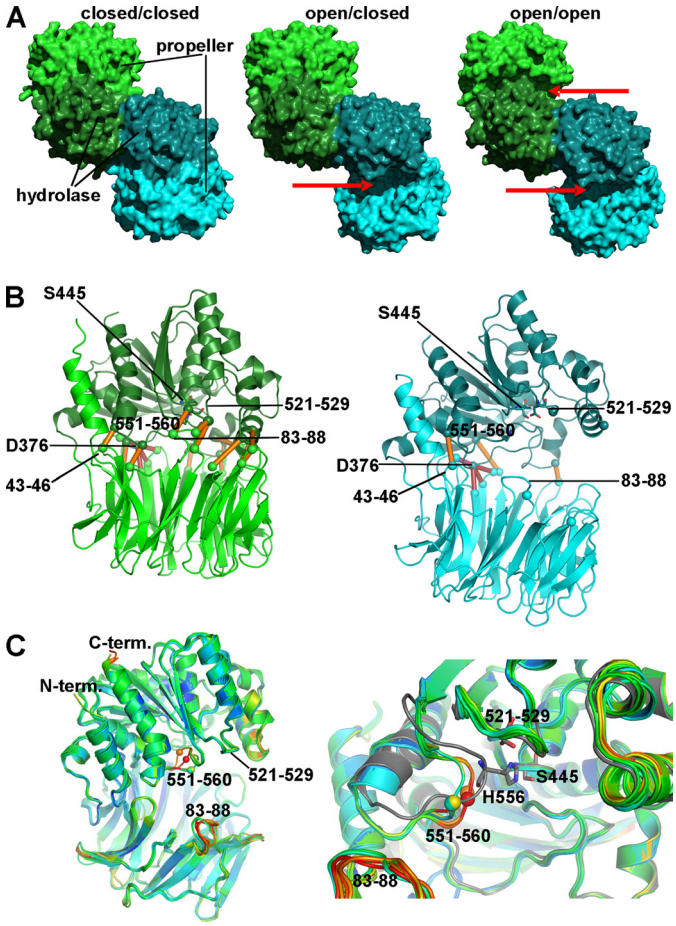

FIGURE 5. **Overall conformation of the ApAAP structures.** *A*, molecular surface representation of the known ApAAP dimer structures (monomers are shown in *blue* and *green*; hydrolase domains are in *darker colors*). Previously published structures (PDB ID codes 1VE6, 1VE7, 2HU5, 2HU7, and 2HU8) show the closed/closed conformation. Three of the present structures are in the open/closed conformation (the interdomain opening is marked with a *red arrow*), and one is in the open/open conformation. *B*, Cα-Cα distances of residues involved in interdomain hydrogen bonds are marked with *orange lines*, whereas those in the hinge region are represented with *red lines*. Most of the hydrogen bonds of the closed structure (*left*) are broken in the open structure (*right*); in contrast, the hydrogen bonds of Asp^{376} (hinge region, *red lines*) are preserved. *C*, the superposition of the open structures reveals their similarity (all eight of the open monomers of the four crystal structures are shown). The schematic representations of the open structures are color-ramped *blue* to *red* from low to high residual B-factors. *Left*, loop-(83–88) and loop-(551–560) (containing the catalytic His^{556}) show high mobility in all of the open structures. *Right*, the conformation of the loop containing His^{556} (Cα atom shown with a *sphere*) is also changed significantly. The closed structure is shown in *gray* as reference with the catalytic triad in *stick* representation.

formation; its side chain could only be detected in the electron density map in four of the eight crystallographically independent open state monomers. However, in those open conformation structures, the guanidinium group forms a double H-bond with Asp^{482} of the hydrolase domain, providing a further example of interdomain to intradomain H-bond switch upon opening (Fig. 6, *A* and *B*).

In the D524N structure, the side chain conformation of Asn^{524} is fixed in a catalytically unfavorable conformation by hydrogen bonds, with its side chain NH_2 group pointing to the direction of His^{556}. Widening of the electron density of the imidazole group of the catalytic His^{556} suggests that the histidine may be in alternate conformations (Fig. 6*D*), possibly because it is partially protonated at the pH of the crystallization condition. Both of these conformations cause the loss of the catalytically essential hydrogen bonds: 1) Either its position is similar to that of the native enzyme, but it is in the wrong tautomeric form (*cf.* the study on trypsin (14)), or 2) the imidazole ring is shifted away from the asparagine residue, causing distortion or even the loss of its hydrogen bond to Ser^{445}. In the latter case, the shift of the histidine is greater than that of the D524A form.

The pH applied at crystallization most probably causes partial protonation of the catalytic His in all structures. The double protonated imidazole group thus becomes proton donor. In the case of the native structure, this simply results in slightly unfavorable H-bonding geometry for the catalytic Ser residue, whereas the members of the catalytic triad remain within H-bonding distance from each other. In the case of the D524A mutant, where a water molecule is bound in place of the Asp carboxylate and the His is shifted further from the Ser, the effect of protonation on the structure of the active site is negligible. The most marked effect can be seen with the D524N mutant. Because the carbonyl oxygen of Asn^{524} is engaged in a hydrogen bond with the backbone NH group of the Arg^{526} residue, its amide group, a proton donor itself, is forced in the direction of His. The protonated His, in the middle of the triad, is an incompatible partner for both the Asn and the Ser and shifts to an even greater extent. However, at alkaline pHs and in the presence of substrates, the canonical serine-histidine interaction may be recovered, which is in line with the different kinetic behaviors of different substrates.

DISCUSSION

Unexpectedly Different Kinetic Behavior of AAP and POP Mutants—In reactions of the D102N trypsin variant, the reduction in the rate constant was independent of the substrate (14, 15), suggesting that site-specific mutagenesis is a useful method for determining the contribution of a functional group to catalysis. In contrast, the fall in the reaction rate with POP exhibited a difference of 6 orders of magnitude between the hydrolysis rates of a nitrophenyl ester and an oligopeptide (16). Significant differences were observed in the reactions of ApAAP as well, using different substrates and mutations (Table 2).

The bell-shaped pH-rate profile obtained with wild-type POP was preserved with the enzyme variants. However, the bell-shaped curve for native ApAAP, which contained one catalytically active form, changed to a double sigmoid or pH-independent curve, implying two active forms located primarily in the acidic and the alkaline pH region, respectively (Fig. 1, *A* and *B*). The activity of the acidic form is controlled by a gradual change in the protonation state of the catalytic histidine residue. Throughout the alkaline pH range, the imidazole group must be in the catalytically active, basic form. Therefore, the invariable ionization state of the imidazole cannot be responsible for the increase or decrease in activity. In this pH region, the ionization of other groups and conformational changes may impede (native enzyme) or facilitate (mutant enzymes) the reaction. The rate constant for the D102N mutant of trypsin also increased in the alkaline pH

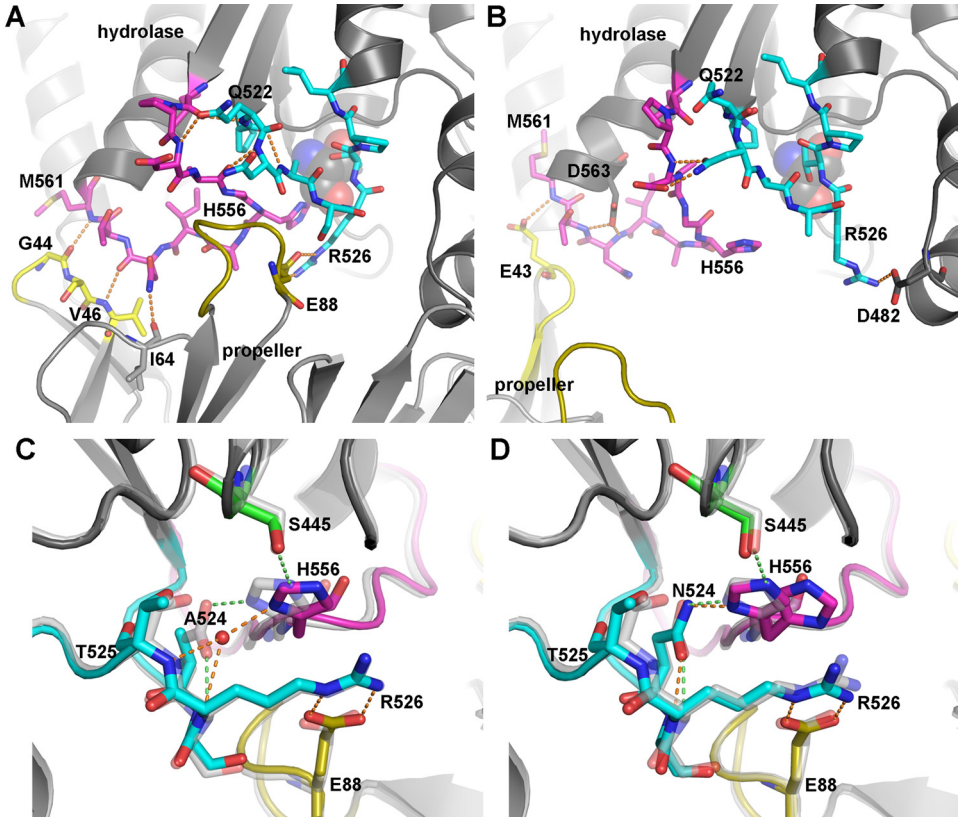

FIGURE 6. **Rearrangement of the active site caused by structure opening or the D524A and D534N mutations.** Conformations and hydrogen bond networks of the loops holding the active site residues in the closed and open structures are shown in *A* and *B*, respectively. Loop-(551–560) holding His^{556} and loop-(521–529) holding Ala^{524} are shown in *magenta* and *cyan*, respectively. Ser^{445} is shown with *spheres* in the background. The propeller domain is shown in *lighter gray* with loops 43–46 and 83–88 in *yellow*. Note that the conformation and interactions of loop-(521–529) are similar in the mutant and native forms, whereas those of loop-(551–561) vary. *C* and *D* show the effect of mutation on the active site of the closed, intact structures. *C*, superposition of the D524A mutant and wild-type structures. *D*, superposition of the D524N mutant and wild-type structures. The catalytic histidine is in dual conformation. The loops of the mutant forms are colored as on *A* and *B*. Ser^{445}, *green* with *orange* hydrogen bonds. The native structure is transparent *gray* with *light green* hydrogen bonds. Although the backbone conformation is unchanged in the mutant forms, the His^{556} side chain is rotated in a catalytically less favorable position, and the Ser-His hydrogen bond is lost. The distortion effect is more enhanced in the D524N form.

region. This phenomenon was interpreted in terms of participation either of a titratable base or of In case of a hydroxide ion in the catalytic mechanism (15). The progressive increase of the rate constant between pH 8 and 10 was also observed with subtilisin mutated at the catalytic histidine, and the rate enhancement was attributed to hydroxide ion catalysis (45). With very poor enzymes such as the His^{64} mutant of subtilisin or with substrates having a relatively good leaving group, the hydroxide ion catalysis is conceivable. However, with the stable peptide bond as found in the present study on ApAAP (Fig. 1*B*) a progressive structural change must be preferred to the hydroxide ion catalysis in the alkaline pH range.

Significant differences were also found between the association constants ($1/K_i$) of product-like inhibitors for POP and ApAAP. Thus, the benzyloxycarbonyl-Gly-Pro-OH binding weakens with the POP variants (D641A and D641N), and the titration curves do not point to participation of the catalytic histidine in binding, whereas the imidazole of the wild-type POP is properly titrated (16). The wild-type ApAAP is also well titrated with Ac-Phe-OH. Distinct from the corresponding POP reactions, the inhibitor binding to the D524N variant of ApAAP is similar to that observed with the wild-type enzyme, but the D524A variant is not titrated (Fig. 4). This unexpected behavior of the D524A mutant is consistent with the pH-independent pH-rate profile (Fig. 2). In the crystal structure of the D524A mutant, the catalytic imidazole group is pushed by a water molecule 0.7 Å further from Ser^{445} than it is in the wild-type structure and moves closer to Arg^{526}. The main structural effects unfavorable for catalysis are: the loss of the negative charge of the aspartate; the distortion of the serine-histidine hydrogen bond; and the closeness of a positively charged group with the histidine, which is also positively charged during the reaction process.

In the D524N mutant form, a further unfavorable effect takes place on the hydrogen bond network. The side chain of Asn occupies exactly the same position as the Asp^{524} side chain in the native structure. However, its amide NH_2 group points toward the active His^{556}, which can either assume a catalytically noncompetent tautomeric form or shift away from Ser^{445} (Fig. 6*D*). In contrast, in the corresponding D641N variant of POP, it is the loop holding residue 641 that is rearranged (16). The differences in the Ac-Phe-OH binding kinetics of the two mutant ApAAP forms may be explained by the different distortions of the catalytic histidine.

The dissociation constant of the enzyme-substrate complex (K_s) is also distinctly affected by the mutation on POP and ApAAP. Specifically, the K_s is about four times higher for the wild-type POP than for its D641A variant, while the K_s values

are similar for the wild-type ApAAP and its variants. The K_m values of the reaction of oligopeptide with the three kinds of ApAAP are also similar and are close to K_s, as occurs in the case of the true Michaelis-Menten mechanism. On the other hand, the Ac-Phe-Nap reaction follows the Briggs-Haldane mechanism, where $K_m = K_s + k_2/k_1$ is greater than K_s by k_2/k_1.

Mechanism of Oligopeptidase Activity—In the POP family, the active site of an enzyme is located in a cavity between the two domains of the enzyme. Although with some enzymes, like DPP-IV (46–48), the oligopeptides of restricted size can access the active site through a stable, sufficiently large opening, for other members of the family (*e.g.* POP and AAP) the closed structures do not allow the substrate to access the binding site and the catalytic residues. In this latter case, a dynamic opening between the two domains is necessary for the substrate to enter the active site (17).

Such an open conformation was observed in the crystal structure of the monomer POP from *Sphingomonas capsulata* (PDB ID code 1YR2). In that case the C-terminal His_6 tag of one molecule intrudes into the interface region between the two domains of another molecule (49); thus the closed conformation of that enzyme could not be determined.

Very recently, the structure of *Aeromonas punctata* POP has also been determined (50). The authors concluded that the flexible open form of the enzyme is its resting state and that the binding of inhibitors or substrates initiates the closing by an induced-fit mechanism.

Our results indicate that the substrate-induced mechanism for closing is not universal in the oligopeptidase family, because the open and closed forms are present in the crystal in the absence of substrate and may co-exist in solution. Contrary to the previous findings for ApAAP crystals that contained two closed subunits (24, 25), in the present work, using very similar crystallization protocols we have obtained distinct crystal forms having one closed and one open molecule in the dimer enzyme and an open/open dimer structure. Both the native and mutant enzymes displayed mixed subunits, and this fact indicates that opening of the structure is not a consequence of the mutations. The structures of the two states obtained simultaneously provided a unique framework for studying the conformational variations during opening and closing. The results demonstrate that the opening of the enzyme leads to the breakdown of the catalytic triad, whereas closing rearranges these changes.

The fact that nearly identical open conformations were observed in four different crystal forms suggests that the open and closed forms of ApAAP are the major, stable species of similarly low energy. In contrast, with the *A. punctata* POP (50) an array of co-existing, transitionally opened states was found in almost identical crystal lattices.

The opening of the ApAAP structure is similar to the opening of a clamshell. The hinge region is centered on the Asp^{376} residue of the hydrolase domain, which forms five interdomain H-bonds that are retained in the open form. In the case of the *A. punctata* POP, no such stabilizing hinge point was detected, which may account for the observed various extents of opening (50). In the closed form of ApAAP, the loops between the hydrolase and the propeller domains form an extensive network of further interdomain H-bonds in addition to the five with Asp^{376}, approximately twice as many as found in the porcine brain POP (PDB ID code 1H2W) or the *A. punctata* POP (PDB ID code 3IVM), which break up on opening. Loop-(521–529) and loop-(551–560) of ApAAP, which contain Asp^{524} and His^{556}, respectively, contribute to the stabilization of the closed conformation of the enzyme forming hydrogen bonds with the propeller domain.

In ApAAP, the domain surfaces that become solvent-exposed by the opening are composed of nearly as many hydrophobic as hydrophilic residues (55 *versus* 45%, respectively). This, taken together with the fact that the open and closed forms crystallized in a 1:1 ratio in three cases, suggests that although a great number of the original H-bonding contacts are lost in the open form, hydration of the polar residues must compensate for the loss of energy. During closing, the reformation of the original hydrogen bonds and hydrophobic contacts compensates for dehydration of the polar residues. The fast equilibrium between the open (substrate accessible) and closed (active) forms is supported by the fact that the enzyme is a very effective catalyst, as indicated by its high k_{cat}/K_m of about 8 $\mu M^{-1}s^{-1}$. Note that some transient form may also participate in substrate binding. In the case of the *A. punctata* POP, the solvent-exposed domain interfaces of the open form consist mostly (70%) of polar or charged residues, shifting the equilibrium toward the open form, which is postulated as the resting state of the enzyme (50). On the other hand, ligand-free porcine brain POP was crystallized in the closed form, suggesting that the relative stability of the open and closed forms in their equilibrium may vary even among related enzymes of the POP family. This equilibrium can be modulated by fine effects, most likely by the amino acid composition of the domain interfaces.

The binding of substrate or inhibitor must facilitate the closing, because the bound ligands cross-link the peptidase and the propeller domains. In the case of AAP, the P1 residue of the substrate is bound to the hydrolase domain, and the P2 and P3 residues are anchored to the propeller through the Arg^{526}-Glu^{88} ion pair and the hydrophobic residues of the S3 subsite (Leu^{115}, Phe^{153}, and Phe^{155}), respectively (25).

The three amino acids of the catalytic triad (Ser^{445}, Asp^{524}, and His^{556}) are members of a short turn and two loops, which are brought into proximity by the fold of the hydrolase domain. The two regions that undergo the greatest rearrangements in the open state are two loops forming a buckle in the closed state, *i.e.* loop-(43–46) of the propeller and loop-(551–560) of the hydrolase domain. The rearrangement of loop-(551–560) bearing the His^{556} residue is of functional significance, because restructuring of this loop during opening leads to disassembly of the catalytic triad. Ser^{445} is located in a tight turn between a β-strand and a helix, positioned by four specific backbone H-bonds, and is not perturbed by the opening. Loop-(521–529), containing the active Asp^{524}, is shifted only moderately upon opening; therefore, the 3.4–5.0 Å Cα shift of His^{556} results in the breakup of the active site triad. The opening also enhances the conformational freedom of the two loops, especially of loop-(551–560), without increasing the

flexibility of the catalytic serine. Thus, our results show that while the α/β hydrolase fold ensures the spatial proximity of the active site residues, their stabilization and correct positioning is completed only by the interdomain contacts in the closed state.

Inactivation of the open state proceeds in a different way with the *A. punctata* POP (50). The explanation was focused on an Arg residue of the hydrolase domain, which, in the active, closed state participates in substrate binding. This residue forms an interdomain double H-bond with an Asp of the propeller region. The authors (50) found that this Arg residue in the various open forms intrudes between members of the catalytic triad, fixing either the Ser or the Asp in an unfavorable conformation. In the case of ApAAP, the corresponding Arg^{526} similarly forms an interdomain association with conserved Glu^{88} in the closed form. However, in the open state, instead of interacting with the active site residues, Arg^{526} forms an intradomain association with Asp^{482} (Fig. 6, *A* and *B*). Asp^{482} is also conserved among vertebrate AAPs, but in the *A. punctata* POP, a Thr residue is found in the same position. There are two further differences between the POP and ApAAP. First, the loop containing the catalytic histidine residue is not seen in the electron density map of POP, which indicates higher conformational flexibility. Second, a ligand-free, active, closed structure of POP was not crystallized, so that the structural basis of the conformational changes could not be defined.

The open and closed structures of ApAAP differ in the catalytic sites, with only the closed form being active, whereas the open form exhibits inactive conformation. This implies that the enzyme is unable to cleave the peptide bond in the open form. Therefore, the hydrolysis of a disordered large peptide may not occur even if it binds to the distorted active site. However, several papers have indicated that some serine oligopeptidases hydrolyze large proteins. For example, fibroblast activation protein has gelatinase and collagenase activities (51), oligopeptidase B cleaves at a restricted site of histone proteins (52), and POP digests itself (53, 54) or degrades a splice variant protein of p40-phox (55). In all of these cases the hydrolytic reactions require unusually long times, at least overnight. Being extremely slow, the specificity rate constants were not determined so the hydrolytic reactions in this case cannot be considered as normal enzyme reactions.

Conclusion—The exact role of Asp in the catalytic triad of serine peptidases has not yet been clearly established. Here we investigated the kinetics and the structures of two mutant enzymes in which the catalytic aspartic acid was changed (D524N and D524A). The pH-k_{cat}/K_m profile of ApAAP and its variants proved to be very different. Also, the pH dependence of the association constant obtained from titration with the Ac-Phe-OH inhibitor has shown that the participation of the catalytic histidine is different in the reactions of different ApAAP variants. Similar mutations with POP led to kinetic results that differed in several aspects from those found with ApAAP. Thus, the change in catalysis on mutation depends considerably on both the kind of mutation and the nature of the substrate. The present results, as well as those obtained previously with POP mutants, imply that the negative charge

$$E^{c,i} \leftrightarrows E^{o,i} + S \rightarrow ES^{c,a} \rightarrow EA^{c,a} + P_1 \rightarrow E^{o,i} + P_2$$

SCHEME 2

on the Asp residue is essential for stabilizing the reaction intermediates and that site-specific mutagenesis does not necessarily reflect the intrinsic contribution of a functional group to catalysis. The kinetic results are consistent with the crystal structure determinations, illustrating the alterations in the position of the catalytic His of the enzyme variants, even in conservative substitution, and this points to an important role of Asp in orienting the catalytic His.

The catalytic mechanism may follow that shown in Scheme 2, where *c*, *o*, *i*, and *a* represent the closed, open, inactive, and active forms of ApAAP, respectively. *E*S, *E*A, P1, and P2 stand for the enzyme-substrate complex, the acyl-enzyme, product 1, and product 2, respectively.

It may be noted that the first enzyme-substrate complex is generated with the open, inactive enzyme form ($ES^{o,i}$). However, this is not a well defined species; the substrate is not at a catalytically competent place. It assumes the final position in the closed, active enzyme form ($ES^{c,a}$). According to Scheme 2, the closed and open states are at equilibrium. Both forms are inactive, because the closed form cannot accept the substrate and the catalytic triad is damaged in the open form. The formation of *E*S goes along with closing, and this is followed by acylation and deacylation. This mechanism is at variance with the induced-fit mechanism published recently for *A. punctata* POP (50); that proposal implies that the enzyme exists in the open state, and the addition of substrate induces large conformational change into the closed state with induced-fit adjustments of the active site. In the absence of substrate or inhibitor, POP does not assume its closed form, as all POPs contained substrate or inhibitor when crystallized in the closed form (50). However, we have obtained closed porcine POP crystals several times that displayed a catalytically active conformation even without substrate or inhibitor ligand. This observation raises the possibility that the closely related enzymes, POP and ApAAP, operate via similar mechanisms, which implies conformational selections consistent with the classical model pioneered by Monod, Wyman, and Changeux (the MWC model). This paradigm, in recent years, has been preferred to the induced-fit mechanism (*cf.* for example Ref. 56).

Acknowledgments—We thank Dr. Paul Tucker (EMBL, Hamburg, Germany) and Dr. Alberto Cassetta (ELETTRA, Trieste, Italy) for help during data collection. Access to EMBL beamlines X11 and X12 at the DORIS storage ring, DESY, Hamburg, as well as beamline XRD1 at ELETTRA Synchrotron, Trieste, is gratefully acknowledged.

REFERENCES

1. Polgár, L. (1989) *Mechanisms of Protease Action*, Chapter 3, pp. 87–122, CRC Press, Boca Raton, FL
2. Hedstrom, L. (2002) *Chem. Rev.* **102,** 4501–4524
3. Polgár, L. (2005) *Cell. Mol. Life Sci.* **62,** 2161–2172
4. Blow, D. M., Birktoft, J. J., and Hartley, B. S. (1969) *Nature* **221,** 337–340
5. Polgár, L., and Bender, M. L. (1969) *Proc. Natl. Acad. Sci. U.S.A.* **64,**

1335–1342
6. Bachovchin, W. W., Kaiser, R., Richards, J. H., and Roberts, J. D. (1981) *Proc. Natl. Acad. Sci. U.S.A.* **78,** 7323–7326
7. Jordan, F., and Polgár, L. (1981) *Biochemistry* **20,** 6366–6370
8. Kossiakoff, A. A., and Spencer, S. A. (1981) *Biochemistry* **20,** 6462–6474
9. Polgár, L. (1972) *Acta Biochim. Biophys. Acad. Sci. Hung.* **7,** 29–34
10. Fersht, A. R., and Sperling, J. (1973) *J. Mol. Biol.* **74,** 137–149
11. Warshel, A. (1978) *Proc. Natl. Acad. Sci. U.S.A.* **75,** 5250–5254
12. Warshel, A., Naray-Szabo, G., Sussman, F., and Hwang, J. K. (1989) *Biochemistry* **28,** 3629–3637
13. Carter, P., and Wells, J. A. (1988) *Nature* **332,** 564–568
14. Sprang, S., Standing, T., Fletterick, R. J., Stroud, R. M., Finer-Moore, J., Xuong, N. H., Hamlin, R., Rutter, W. J., and Craik, C. S. (1987) *Science* **237,** 905–909
15. Craik, C. S., Roczniak, S., Largman, C., and Rutter, W. J. (1987) *Science* **237,** 909–913
16. Szeltner, Z., Rea, D., Juhász, T., Renner, V., Mucsi, Z., Orosz, G., Fülöp, V., and Polgár, L. (2002) *J. Biol. Chem.* **277,** 44597–44605
17. Fülöp, V., Böcskei, Z., and Polgár, L. (1998) *Cell* **94,** 161–170
18. Naylor, S. L., Marshall, A., Hensel, C., Martinez, P. F., Holley, B., and Sakaguchi, A. Y. (1989) *Genomics* **4,** 355–361
19. Scaloni, A., Jones, W., Pospischil, M., Sassa, S., Schneewind, O., Popowicz, A. M., Bossa, F., Graziano, S. L., and Manning, J. M. (1992) *J. Lab. Clin. Med.* **120,** 546–552
20. Erlandsson, R., Boldog, F., Persson, B., Zabarovsky, E. R., Allikmets, R. L., Sümegi, J., Klein, G., and Jörnvall, H. (1991) *Oncogene* **6,** 1293–1295
21. Yamaguchi, M., Kambayashi, D., Toda, J., Sano, T., Toyoshima, S., and Hojo, H. (1999) *Biochem. Biophys. Res. Commun.* **263,** 139–142
22. Duysen, E. G., Li, B., Xie, W., Schopfer, L. M., Anderson, R. S., Broomfield, C. A., and Lockridge, O. (2001) *J. Pharmacol. Exp. Ther.* **299,** 528–535
23. Richards, P. G., Johnson, M. K., and Ray, D. E. (2000) *Mol. Pharmacol.* **58,** 577–583
24. Bartlam, M., Wang, G., Yang, H., Gao, R., Zhao, X., Xie, G., Cao, S., Feng, Y., and Rao, Z. (2004) *Structure* **12,** 1481–1488
25. Kiss, A. L., Hornung, B., Rádi, K., Gengeliczki, Z., Sztáray, B., Juhász, T., Szeltner, Z., Harmat, V., and Polgár, L. (2007) *J. Mol. Biol.* **368,** 509–520
26. Kiss, A. L., Szeltner, Z., Fülöp, V., and Polgár, L. (2004) *FEBS Lett.* **571,** 17–20
27. Leatherbarrow, R. J. (2001) *Grafit*, Version 5.0, Erithacus Software Ltd., Horley, UK
28. Segel, I. H. (1975) *Enzyme Kinetics*, pp. 72–74, John Wiley & Sons, Inc., New York
29. Kabsch, W. (1993) *J. Appl. Crystallogr.* **26,** 795–800
30. Vagin, A. A., and Treplyakov, A. (1997) *J. Appl. Crystallogr.* **30,** 1022–1025
31. Murshudov, G. N., Vagin, A. A., and Dodson, E. J. (1997) *Acta Crystallogr. D Biol. Crystallogr.* **53,** 240–255
32. Winn, M. D., Isupov, M. N., and Murshudov, G. N. (2001) *Acta Crystallogr. D Biol. Crystallogr.* **57,** 122–133
33. Emsley, P., and Cowtan, K. (2004) *Acta Crystallogr. D Biol. Crystallogr.* **60,** 2126–2132
34. Laskowski, R. A., MacArthur, M. W., Moss, D. S., and Thornton, J. M. (1993) *J. Appl. Crystallogr.* **26,** 283–291
35. Berman, H. M., Westbrook, J., Feng, Z., Gilliland, G., Bhat, T. N., Weissig, H., Shindyalov, I. N., and Bourne, P. E. (2000) *Nucleic Acids Res.* **28,** 235–242
36. DeLano, W. L. (2002) *The PyMOL Molecular Graphics System*, DeLano Scientific, San Carlos, CA
37. Reynolds, C., Damerell, D., and Jones, S. (2009) *Bioinformatics* **25,** 413–414
38. Fersht, A. (1998) *Structure and Mechanism in Protein Science*, Chapter 3, pp. 103–131, W. H. Freeman and Co., New York
39. Polgár, L. (1999) in *Proteolytic Enzymes: Tools and Targets* (Sterchi, E. E., and Stöcker, W., eds) pp. 148–166, Springer-Verlag, Berlin
40. Wang, Q., Yang, G., Liu, Y., and Feng, Y. (2006) *J. Biol. Chem.* **281,** 18618–18625
41. Zerner, B., Bond, R. P., and Bender, M. L. (1964) *J. Am. Chem. Soc.* **86,** 3669–3674
42. Polgár, L. (1992) *Biochem. J.* **283,** 647–648
43. James, M. N., Sielecki, A. R., Brayer, G. D., Delbaere, L. T., and Bauer, C. A. (1980) *J. Mol. Biol.* **144,** 43–88
44. Fülöp, V., Szeltner, Z., Renner, V., and Polgár, L. (2001) *J. Biol. Chem.* **276,** 1262–1266
45. Carter, P., and Wells, J. A. (1987) *Science* **237,** 394–399
46. Engel, M., Hoffmann, T., Wagner, L., Wermann, M., Heiser, U., Kiefersauer, R., Huber, R., Bode, W., Demuth, H. U., and Brandstetter, H. (2003) *Proc. Natl. Acad. Sci. U.S.A.* **100,** 5063–5068
47. Rasmussen, H. B., Branner, S., Wiberg, F. C., and Wagtmann, N. (2003) *Nat. Struct. Biol.* **10,** 19–25
48. Hiramatsu, H., Kyono, K., Higashiyama, Y., Fukushima, C., Shima, H., Sugiyama, S., Inaka, K., Yamamoto, A., and Shimizu, R. (2003) *Biochem. Biophys. Res. Commun.* **302,** 849–854
49. Shan, L., Mathews, I. I., and Khosla, C. (2005) *Proc. Natl. Acad. Sci. U.S.A.* **102,** 3599–3604
50. Li, M., Chen, C., Davies, D. R., and Chiu, T. K. (2010) *J. Biol. Chem.* **285,** 21487–21495
51. Park, J. E., Lenter, M. C., Zimmermann, R. N., Garin-Chesa, P., Old, L. J., and Rettig, W. J. (1999) *J. Biol. Chem.* **274,** 36505–36512
52. Morty, R. E., Fülöp, V., and Andrews, N. W. (2002) *J. Bacteriol.* **184,** 3329–3337
53. Harwood, V. J., Denson, J. D., Robinson-Bidle, K. A., and Schreier, H. J. (1997) *J. Bacteriol.* **179,** 3613–3618
54. Harris, M. N., Madura, J. D., Ming, L. J., and Harwood, V. J. (2001) *J. Biol. Chem.* **276,** 19310–19317
55. Hasebe, T., Hua, J., Someya, A., Morain, P., Checler, F., and Nagaoka, I. (2001) *J. Leukoc. Biol.* **69,** 963–968
56. Boehr, D. D., Nussinov, R., and Wright, P. E. (2009) *Nat. Chem. Biol.* **5,** 789–796